CGS Based Solar Cells with In_2S_3 Buffer Layer Deposited by CBD and Coevaporation

W. Vallejo* and J. Clavijo
Departamento de Química, Universidad Nacional de Colombia

G. Gordillo
Departamento de Física, Universidad Nacional de Colombia, Bogotá, Colombia.
(Received on 29 August, 2009)

In this paper we investigated In_2S_3 as substitute for CdS, which is conventionally used as buffer layer in chalcopyrite based solar cells. In_2S_3 thin films were deposited by CBD and co-evaporation methods and these were employed as buffer layer in $CuGaSe_2$ based solar cells. Previous to the device fabrication, comparative study was carried out on In_2S_3 thin films properties deposited from chemical bath containing thioacetamide, Indium Chloride, and sodium citrate, and In_2S_3 thin films prepared by co-evaporation from its constituents elements. The influence of synthesis conditions on the growth rate, optical, structural and morphological properties of the as-grown In_2S_3 thin films have been carried out with Spectrophotometry, X-ray diffraction and AFM microscopy techniques. Suitable conditions were found for reproducible and good quality In_2S_3 thin films synthesis. By depositing In_2S_3 thin films as buffer layers in $CuGaSe_2$ configuration, a maximum solar cell efficiency of 6% was achieved, whilst the reference solar cell with $CdS/CuGaSe_2$ on similar absorber exhibited 7% efficiency.

Keywords: Buffer layer, In_2S_3, CBD, chalcopyrite, structural properties, Solar cell.

1. INTRODUCTION

In most laboratories the standard device structure of $Cu(In,Ga)Se_2$ (CIGS)-based solar cells includes a very thin chemical-bath-deposited (CBD) CdS buffer layer between the CIGS absorber layer and the transparent ZnO front electrode. At present the best results obtained with thin film based solar cells, have been achieved with solar cells fabricated using the structure Mo/CIGS/CdS/ZnO; the maximum efficiency reported for this type of devices is 19.9% [1]. In the last decade, serious efforts to substitute the CdS buffer layer by other nontoxic materials have been made for the following reasons:

i) The expected environmental risks arising from implementation of synthesis CdS thin film by CBD process in a CIGS module production line.

ii) The possibility to improve the light transmission in the blue wavelength region by using a material with a wider bandgap compared to CdS.

Alternative buffer layers to CdS films have been investigated to fabricate Cd-free devices and enhance solar cell current generation. ZnS-based buffer layers, prepared by CBD and atomic layer deposition (ALD), have already demonstrated their potential as alternative buffer material [2,3]; efficiencies up to 18.6 % have been obtained using ZnS(O,OH)/ZnO as window layer in CIGS based cells [4]. In_2S_3, In_2Se_3, ZnSe and $(Zn,In)Se_x$ layers deposited by different methods have demonstrated to be potential as alternatives buffer layers in chalcopyrite based solar cells [5]. Efficiencies up to 15.7% have been reported to In_2S_3-CBD/CIGS based solar cells [6]. The best results obtained to Cd-free buffer layer in CIGS based cells using materials deposited by physical methods have been achieved using In_2Se_3 and $(Zn,In)Se_x$ [7,8]; efficiencies up to 15.3 % have been reported with $(Zn,In)Se_x$ deposited by co-evaporation in CIGS based cells [8].

In this paper we have deposited good quality In_2S_3 thin films by the CBD method, in this process were used thioacetamide, Indium Chloride and sodium citrate as reagents. On the other hand, we have also found conditions for reproducible deposition of good quality In_2S_3 thin films by co-evaporation from elementals Indium and sulphur. A comparative study of the optical, structural and morphological properties of the In_2S_3 films deposited by both methods is also reported in this work. Preliminary results revealed that the performance of solar cells fabricated with structure SLG/Mo/$CuGaSe_2$/In_2S_3/ZnO/Al is similar to reference solar cell with CdS/$CuGaSe_2$

2. EXPERIMENTAL

In this work the In_2S_3 thin films were prepared by CBD and co-evaporation methods; special emphasis was put on finding conditions to grow In_2S_3 thin films by CBD with adequate properties to be used as buffer layers in $CuGaSe_2$ (CGS) based solar cells. Different layers constituting the device were deposited as follows: The samples prepared by CBD were grown from solution containing Thioacetamide (Scharlau) (TA) and Indium Chloride ($InCl_3$) as sources of S^{2-} and In^{3+} respectively, acetic acid (Es-Science) (HA) and sodium citrate (Riedel-de Han) (Cit) was used as complexing agents of the In^{3+}. the $InCl_3$ was prepared in our laboratory using the following procedure: 67 ml of concentrated HCl and 5 drops of concentrated HNO_3 were added to 22.96 gr (0.200 moles) of metallic In (99.9%, Merck). This solution was heated up until the indium was totally dissolved and the excess HCl evaporated. The resulting solution was diluted to 100mL with water distillated. The In_2S_3 thin films were grown on CGS absorbers and Indium tin oxide covered glass substrates (Kintec Co) (ITO).

The In_2S_3 thin films grown by physical method were obtained by co-evaporation from Indium and Sulphur on CGS and soda lime glass substrates at temperature between 150-450°C. The deposition system is constituted by an evaporation chamber which includes: a tungsten boat for the Indium

*Electronic address: wavallejol@unal.edu.co

evaporation, a tantalum effusion cell for the Sulphur evaporation and a thickness monitor (Maxtec TM-400) with a quartz crystal.

The CGS films were grown by co-evaporation of the precursors in a two stage process [9].

In order to improve the quality of the In_2S_3 films, the preparation parameters were optimized by correlating them with measurements of transmittance, XRD and AFM. These results allowed us to find conditions to grow good quality In_2S_3 thin films. The following chemical bath composition led to good results: [$InCl_3$]=25mM; [TA]=350mM; [HA]=300mM. [Cit]=30mM; during the deposition the bath temperature was maintained at 70°C and the solution pH in 2.5. Additionally Good quality In_2S_3 thin films were obtained by co-evaporation as follows: mass ratio [Sulphur/Indium]=7, Indium deposition rate of 2Å/s, Sulphur evaporation temperature at 140°C and the substrate temperature at 300°C.

The Molybdenum (Mo) films were prepared using a DC magnetron sputtering system with an S-gun configuration electrode. The main difference of this system with the conventional planar Rf sputtering systems, is that the S-gun configuration employs a central anode surrounded by a Mo cathode (99.99% pure), which presents a conical shaped concavity. Details of the Mo films deposition are given in reference [10]. The zinc oxide (ZnO) films were deposited by reactive evaporation using a special procedure described elsewhere [11].

The optical, structural and morphological properties of the In_2S_3 thin films were studied through transmittance, XRD and AFM measurements carried out with a Perkin Elmer Lambda 2S spectrophotometer, an X-ray diffractometer Shimadzu 6000 and a PSI AFM microscope. The film thickness was determined using a Veeco Dektak 150 surface profiler.

3. RESULTS AND DISCUSSION

Previous to the device fabrication, it was performed a comparative study of the deposition conditions influence on the growth rate and on the optical, structural and morphological properties of In_2S_3 thin films CBD and co-evaporated deposited.

3.1. Influence of deposition conditions on the growth rate.

a) In_2S_3 films deposited by CBD

The influence of the preparation method and synthesis parameters on the growth rate and the optical and structural properties of In_2S_3 thin films have been investigated. The variation of the thickness of CBD deposited In_2S_3 thin films as a function of: pH, [TA], [$InCl_3$] and substrate type are plotted in Fig. 1; this study was carried out keeping constant the others parameters as indicated above.

It is observed that the growth rate of the In_2S_3 films is significantly affected by the synthesis parameters and substrate type. Two different regions can be distinguished during the growth process of In_2S_3 thin films (see Fig. 1a), an initial linear region and the final saturation region, which are typical of CBD processes. Before starting the linear growth region, there is a period of time (called induction time), during which is induced the nucleation process which beginning the film growth. The induction time depends on the solution temperature, reagents concentration and substrate type. During the stage of linear growth, the film thickness increases linearly with time; finally, during the saturation stage, the growth rate decreases significantly as consequence of a reduction of the reagents concentration in the solution. Fig. 1a, shows In_2S_3 thin films growth on the two different substrates (ITO and CGS). It is observed that the substrate type significantly affects the growth rate. In general, with the solution we used, the In_2S_3 thin films didn't grow directly on soda lime glass substrates; however, this compound grown quite well on ITO covered glass substrates. It is possible that for starting the nucleation process is required the presence of some ions (Indium and/or tin) on the substrate's surface. On the other hand, the results also show that the layers of In_2S_3 grown faster on CGS than on ITO. This behavior could be explained taking into account that the CBD growth process is affected by surface kinetic processes [12]; in particular, the chemical activity of the substrate surface seems to be the factor responsible for the differences in growth rate observed. The results of Fig. 1a, can therefore be explained assuming that the CGS layers present more chemical activity than ITO covered glass substrate for the CBD growth of In_2S_3 films.

The change of the film thickness as function of molar concentration of the reagents and the pH was studied. Fig. 1b, 1c shows that as the TA and $InCl_3$ concentration increases the thickness of the film increases also. On the other hand Fig. 1(d) shows that growth rate of the processes increases strongly as the pH value decreases. We have found that the optical properties of the In_2S_3 films deposited at pH values lower than 2.0 are poor (low transmittances) whereas those deposited at pH closer to 2.5 present good optical properties. At pH values greater than 2.5 the In_2S_3 films were neither uniforms nor adherents to substrate surface, because under those conditions the homogeneous reaction predominates in the solution. At pH of 2.5 and concentrations [$InCl_3$]=25mM; [TA]=350mM, uniforms layers and adherents to the substrate surface were obtained.

b) In_2S_3 films deposited by co-evaporation

In Fig. 2 are compared curves of thickness vs. deposition time corresponding to In_2S_3 thin films grown by co-evaporation on different substrate types. It is observed that growth rate of In_2S_3 thin films is not affected by neither the substrate type nor the substrate temperature. The results show that unlike In_2S_3 thin films deposited by CBD, the growth rate of In_2S_3 thin films deposited by co-evaporation is independent from type substrate used; it suggests at 300°C the diffusion and coalescence processes occurred at same time on CGS and on soda lime glass substrates. On the other hand the growth rate of In_2S_3 thin films decreases by increasing the substrate temperature, probably due to an increase of the re-evaporation rate of Indium and Sulphur on the substrate surface when the substrate temperature increases.

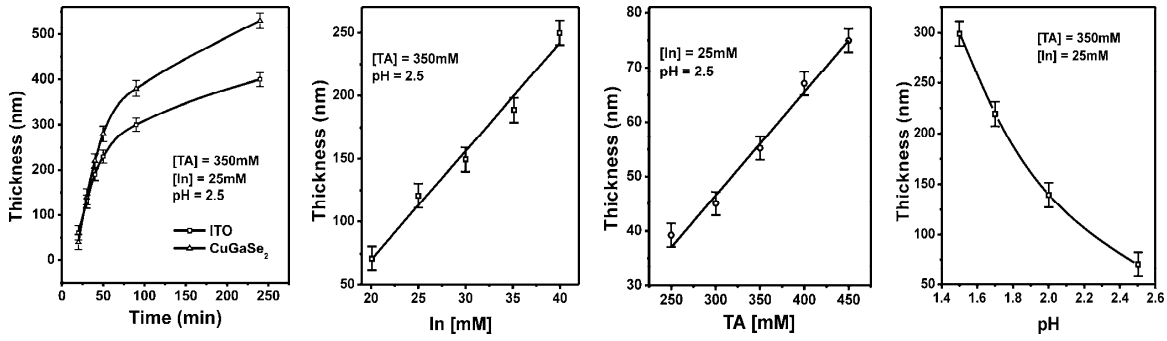

FIG. 1: (a) Change of thickness of In_2S_3 thin films on different substrates as function of deposition time. Change of thickness of In_2S_3 thin films deposited on ITO as function of concentration of: (b) $[InCl_3]$, (c) [TA] and (d) pH.

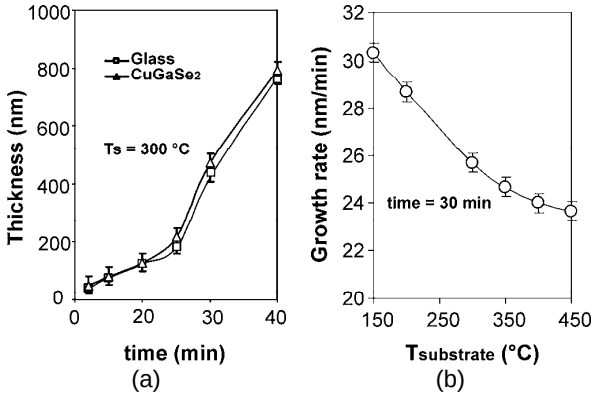

FIG. 2: (a) Change thickness of In_2S_3 thin films grown on different substrates as function of deposition time. (b) Change of growth rate of In_2S_3 thin films grown on glass substrates as function of the substrate temperature.

3.2. Structural results

a) In_2S_3 films deposited by CBD

The In_2S_3 thin films were initially characterized through XRD measurements in order to study the effect of the deposition conditions on the structural properties. Owing to their small thickness, the crystallinity of the films was very poor. The Fig. 3 shows XRD spectra corresponding to In_2S_3 thin films deposited at different molar concentration $InCl_3$ and TA onto ITO substrates, keeping constant the deposition time at 25 minutes and the rest of the deposition parameters as indicated above. Very thin samples deposited at lower $InCl_3$ and TA molar concentrations, present just two reflections at 2θ =33.7 and at 2θ =34.1° which match well reflections associated to the (001) and (200) planes of Indium oxide hydroxide (InOOH) (JCPDS # 17-0549); thicker samples deposited at higher molar concentrations present additionally a third reflection at 2θ =48.37 which match quite well the reflection associated to the (2212) plane of the tetragonal $\beta - In_2S_3$ phase (JCPDS#25-0390).

Some authors have reported results concerning CBD deposited In_2S_3 thin films structure, and most of them suggest a mixture of the cubic α and β phases [13,14]. The presence of Indium oxide hydroxide and another compounds of In_2S_3 such as γ and ε phases have been also reported [14,15]. It seems that the phase in which the CBD deposited In_2S_3 films grow, depends on the deposition conditions, especially type and concentration of the reactants constituting the solution. The fig. 4 shows the XRD pattern corresponding to 80 nm thick In_2S_3 films deposited by CBD on CGS absorber, using a chemical bath composition described above. It is observed that In_2S_3 thin films grown on CGS present the same reflections than samples deposited on ITO substrates, indicating that structure and the phase in which In_2S_3 thin films grow are not affected by substrate type used.

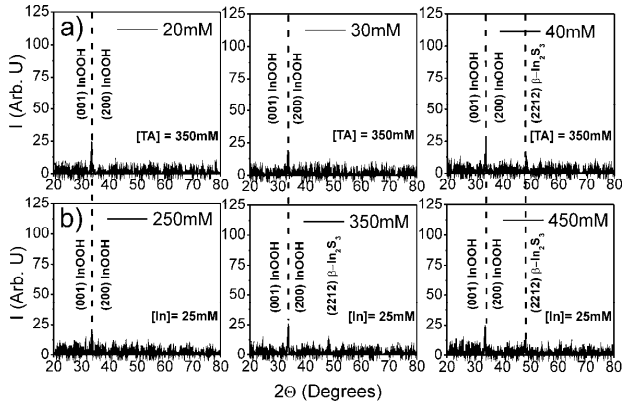

FIG. 3: XRD pattern of In_2S_3 thin films deposited by CBD on ITO for different molar concentration of: (a) $[InCl_3]$, (b) [TA].

b) In_2S_3 films deposited by co-evaporation

Fig. 5 shows experimental XRD pattern corresponding to In_2S_3 thin films deposited on soda lime glass substrates by co-evaporation varying the substrate temperature. The XRD measurements revealed that all the as grown In_2S_3 thin films were polycrystalline in nature; The diffraction peaks could be produced by crystalline planes of the tetragonal $\beta - In_2S_3$ phase (JCPDS # 25-0390), in order to verify this, a XRD pattern theoretically simulated was made (figure 5), the Rietveld method was used in the simulation, and it was assumed that In_2S_3 thin films grown in tetragonal $\beta - In_2S_3$ phase; the sim-

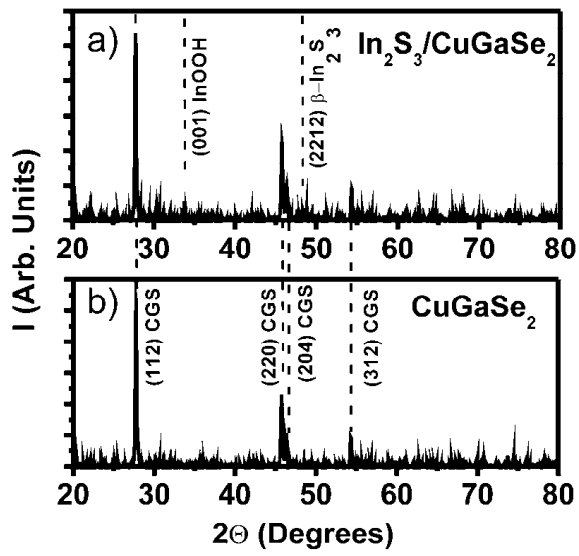

FIG. 4: (a) XRD pattern of 80 nm thick In_2S_3 thin films deposited by CBD on CGS. (b) XRD pattern CGS film.

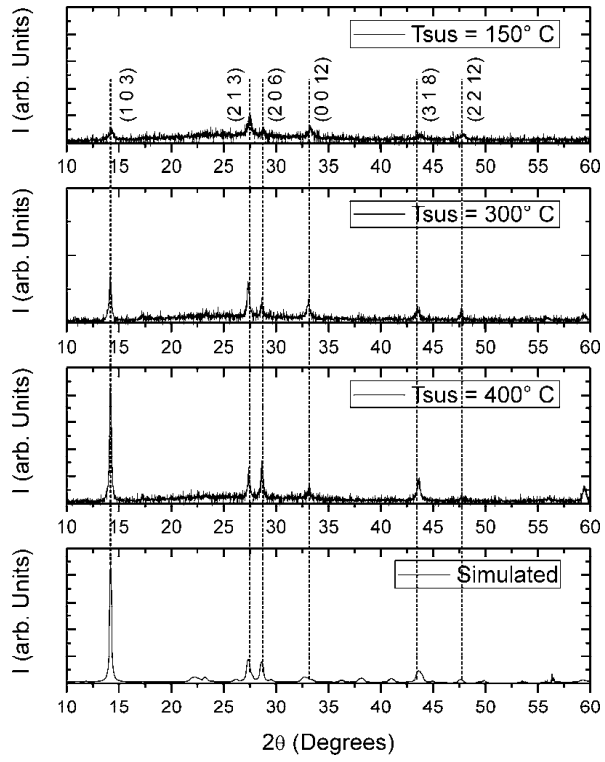

FIG. 5: Comparison of XRD pattern of In_2S_3 thin films deposited by co-evaporation on soda lime glass substrate varying the substrate temperature, with one XRD pattern simulated theoretically assuming that sample grown in the tetragonal $\beta - In_2S_3$ phase.

ulation shows that all reflections resulting from experimental XRD measurements match quite well with reflections of a XRD pattern simulated. These results indicate that $\beta - In_2S_3$ films with adequate properties crystallines for buffer layers can be deposited by co-evaporation at temperatures around 150°C.

The Fig. 6 shows the XRD pattern corresponding to a 110 nm thick In_2S_3 film deposited at 300°C on CGS thin film. The XRD measurements revealed that In_2S_3 films deposited by co-evaporation on CGS films present the same reflections than the samples deposited on glass substrates, indicating that the substrate type does not affect the phase in which In_2S_3 thin film grows.

3.3. Transmittance measurements

a) In_2S_3 films deposited by CBD

Fig. 7 shows typical transmittance curves of In_2S_3 thin films deposited by CBD varying the deposition time and synthesis parameters ([TA], [$InCl_3$], [pH]), keeping constant the rest of deposition parameters as indicated above.

It is observed that the transmittance in the visible region decreases as the concentration of $InCl_3$ increases (fig. 7a), probably due to increasing the film thickness. On the other hand, in the high absorption region (λ<350 nm) the transmittance of layers synthesized at low concentration of TA (fig. 7b), does not reach zero value. This behavior seems to be caused by the presence of pores in the layer of In_2S_3, which are generally formed in very thin films because the amount of reactive is not sufficient to start the coalescence phase of the growth process. This fact prevents the growth of In_2S_3 in some regions of the substrate which facilitates the transmission of light without absorption. On the other hand at pH values lower than 2.0 the optical properties of the films were poor (fig. 7c), the slope of the transmittance

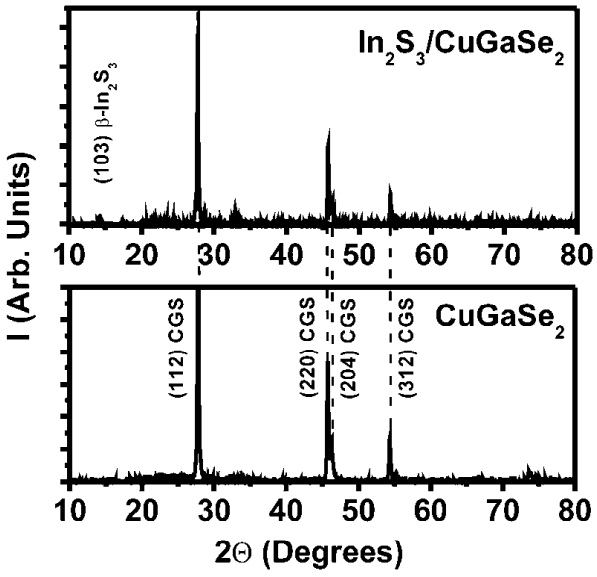

FIG. 6: Comparison of XRD pattern of 110 nm thick In_2S_3 thin film deposited by co-evaporation on $CuGaSe_2$, with the XRD pattern of the $CuGaSe_2$ film.

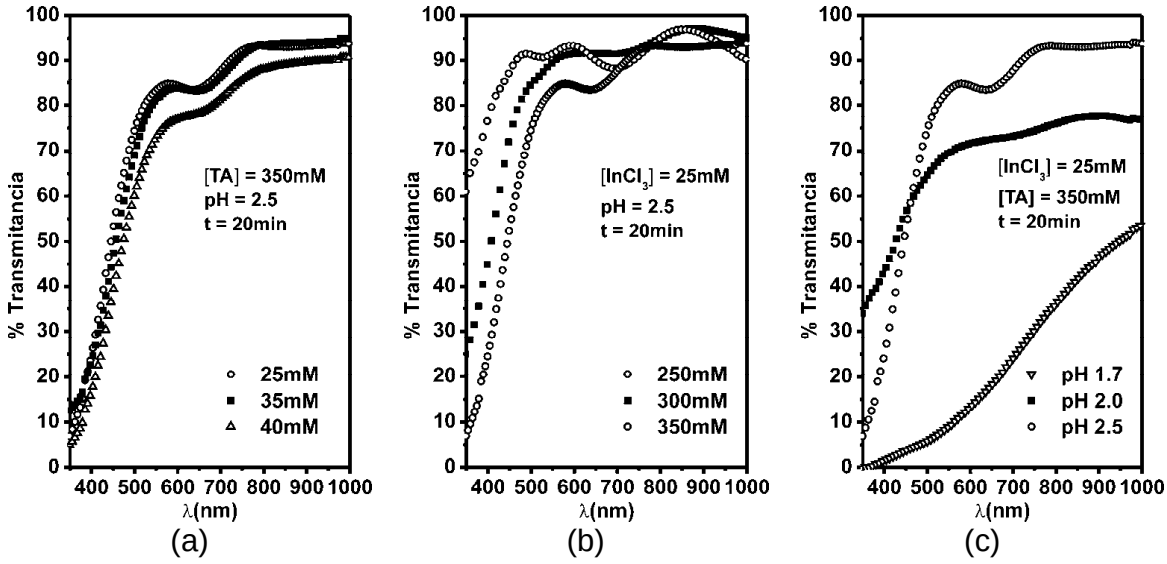

FIG. 7: Change the spectral transmittance of In_2S_3 thin films deposited by CBD on ITO substrates as function of concentration of: (a) $[InCl_3]$, (b) [TA] and (c) pH.

curve and the magnitude of the transmittance are strongly reduced, probably due to the formation of big clusters on the substrate, which are formed as a consequence of strong co-precipitation within the solution of In_2S_3, giving raise to big aggregates that condense on the substrate forming clusters.

b) In_2S_3 films deposited by co-evaporation

In Fig. 8 are plotted typical transmittance curves of In_2S_3 thin films deposited by co-evaporation varying the substrate temperature between 150 and 400°C (Fig. 8a) and the thickness between 80 and 800 nm (Fig. 8b). A curve of $(\alpha h\nu)^2$ vs. $h\nu$, is also shown in Fig. 8c, where α is the absorption coefficient determined from the transmittance measurements and calculations carried out as described in reference [16]; this curve is used for determining the energy band gap Eg of the In_2S_3 thin film, from the intercept with the hν axis of the linear part of the graph $(\alpha h\nu)^2$ vs hν. It is observed a shift of the transmittance curves toward the region of lower values of λ when the thickness decreases. We have not found a definitive explanation for this behavior. However, we consider that the shift of the cutoff wavelength observed could be associated to changes in the band structure, induced by changes in the different interaction processes taking place during stages of the thin films growth. In particular, the superposition degree of electron clouds from neighboring atoms, which affects the band width, can be increased by increasing the film thickness. It was also found that for thicknesses greater than 1 μm, the optical gap of the In_2S_3 thin films keeps constant. Therefore, to prevent the effect of the thickness on the optical gap Eg, a sample with thickness greater than 1 μm was selected to determine this value; an Eg value of 2.75 eV was found for the In_2S_3 film deposited by co-evaporation in this work.

Comparing the transmittance curves of fig. 7b with that displayed in Fig. 8b, it is observed that the transmittance around 350 nm of CBD deposited In_2S_3 films, is significantly lower than those of the In_2S_3 films deposited by co-evaporation, indicating that the substrate-coverage degree of very thin CBD deposited In_2S_3 films is greater than the presented by co-evaporated films with similar thickness. This result indicates that the CBD method allows growing In_2S_3 thin films with larger substrate coverage than samples obtained with similar thickness deposited by co-evaporation.

3.4. Morphological results

a) In_2S_3 films deposited by CBD

Fig. 9 shows typical AFM images of: CGS (Fig. 9a), ITO (Fig. 9b) thin films deposited on soda lime glass substrates, 80 nm thick In_2S_3 thin film deposited by CBD on ITO (Fig. 9c) and CGS (Fig. 9d) thin films respectively. In table 1 are listed the corresponding grain size average values, which were determined analyzing the AFM images showed in Fig. 9, through the ProScan image analysis software. It is observed that the In_2S_3 thin films show similar structure with smaller crystallites that are uniformly distributed over the substrate surface, further the In_2S_3 thin films deposited by CBD on ITO and on CGS covered glass substrates tend to grow with similar morphology and grain size of the substrate on which were grown.

b) In_2S_3 films deposited by co-evaporation

Fig. 10 shows AFM images of In_2S_3 thin films with different thicknesses deposited by co-evaporation on soda lime glass substrate (Fig 10a, b c) and AFM image of In_2S_3 thin film deposited on CGS absorber (Fig 10d). In table 2 are listed the corresponding average values of the grain size and the average surface roughness, obtained for the samples whose AFM images are shown in Fig. 10.

It is observed that the grain size of the In_2S_3 thin films deposited on glass substrates increases significantly when the film thickness increases. At the initial stage of deposition, many nucleation centers present on the substrate and smaller

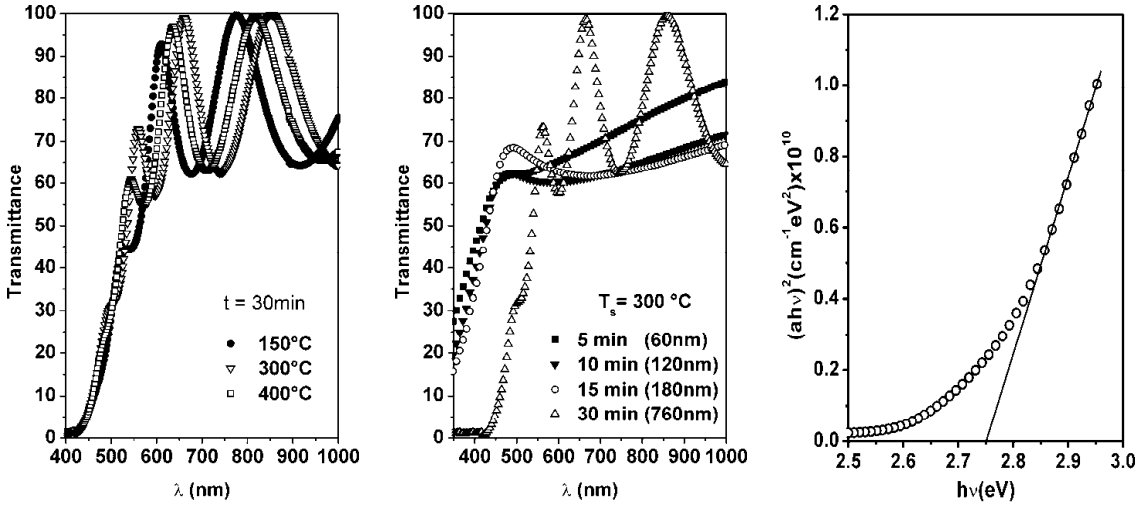

FIG. 8: Change of Spectral transmittance of In_2S_3 thin films deposited by co-evaporation as function of: (a) temperature substrate. (b) deposition time. (c) $(\alpha h\nu)^2$ vs. $h\nu$ spectra indicating the value of Eg.

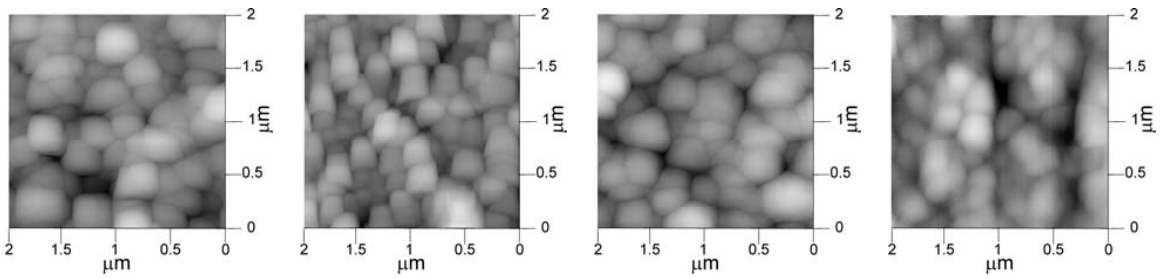

FIG. 9: AFM images corresponding to: (a) CGS substrate, (b) ITO substrate, (c) 80 nm thick In_2S_3 film deposited by CBD on CGS and (d) 80 nm thick In_2S_3 film deposited by CBD on ITO.

TABLE 1: Grain size average values derived from images displayed in Fig. 9.

Sample	Glass/ITO	Glass/$CuGaSe_2$	Glass/CGS/ In_2S_3	Glass/ ITO/ In_2S_3
Grain size (nm)	190	230	215	185

crystallites are produced, for shorter deposition time intervals the films with smaller crystallites are not able to grow into bigger ones (fig.10a), whereas for thicker films (fig.10c) the crystallinity of the film crystallites grew bigger. The AFM measurements also revealed that the In_2S_3 thin films surface topography of the as-grown layers varied with film thickness. The average surface roughness of In_2S_3 films deposited on glass substrate increased from 1.5 nm to 2.5 nm with increase of film thickness (table 2). The increase of surface roughness with thickness is associated with the increase of grain size in the films. However, as film thickness increases the grain size was increased along with the surface roughness, which indicates the 3D growth in the films.

3.5. I-V measurements

The device performance was analyzed by J-V measurements carried out under AM 1.5 irradiance (100 mW/cm^2). Fig. 11 plots J-V curves corresponding to the best CGS based solar cells fabricated with In_2S_3 buffer layer deposited by CBD or co-evaporation, as well as the J-V curve of a reference cell fabricated using a CBD deposited CdS layer as buffer. The In_2S_3 and the CdS buffer layers were deposited on the CGS absorber prepared in the same run with [Ga]/[In]$\sim$ 1.2. In table 3 the output parameters of the best solar cells fabricated using In_2S_3 buffer layers are compared with those of a reference solar cell fabricated with CBD deposited CdS buffer.

In general, the cells fabricated in this work are characterized by rather low open circuit voltage Voc; we observed that in the best case, the Voc/Eg ratio is around 0.47, which is much lower than that of high efficient $Cu(In,Ga)Se_2$ (CIGS) based solar cells with Eg$\sim$1.15 eV, where that ratio is 0.61. It seems the low values of Voc obtained with CGS based cells, are caused by bulk recombination via states generated by intrinsic defects, induced by a lattice mismatch between the surface layer and the bulk material that arises in CGS

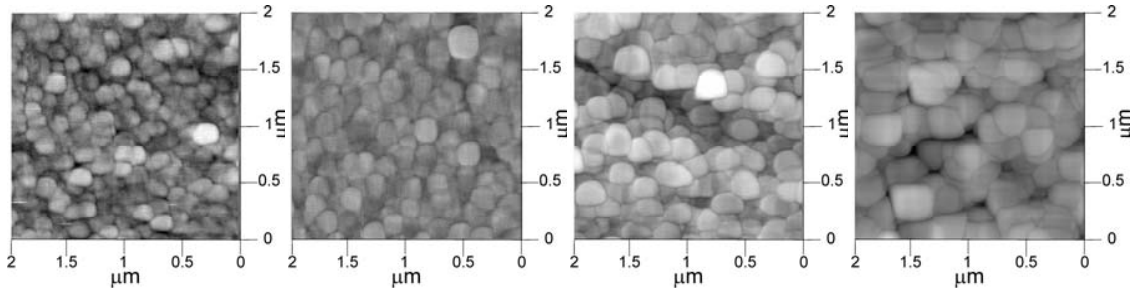

FIG. 10: AFM images of In_2S_3 films deposited by co-evaporation on glass substrates with different film thickness: (a) 110nm, (b) 180 nm, (c) 760 nm. (d) AFM image of a 110 nm thick In_2S_3 film deposited on CGS.

TABLE 2: Grain size average and roughness values derived from images displayed in Fig. 10.

Sample	Glass/ In_2S_3	Glass/ In_2S_3	Glass/ In_2S_3	Glass/CGS/ In_2S_3
In_2S_3 - thickness (nm)	110	180	760	110
Grain size (nm)	110	170	200	210
Roughness Rms (nm)	1.5	2.0	2.5	5.0

at a very high density, as well as in $Cu(In,Ga)Se_2$ alloys with high Ga contents [17]. The increase in bulk recombination leads a decrease in both short circuit current and the electron's diffusion length, which give rise to a decrease of the Voc [18]. Other reason for the large differences in $E_g/q - V_{oc}$ in CGS devices compared with high efficiency CIGS based solar cells, is the increase of the band offset at the absorber/buffer interface by increasing the Ga content of the absorber. It is also observed that the FF of CGS based cells is less than 0.62, which is significantly lower than the efficiency CIGS (> 0.77). The low values of FF of CGS based cells arise as a consequence of high series resistance values ($>10\ \Omega$) and low shunt resistance values ($< 800\ \Omega$).

The results of Fig.11 show that the Voc, Isc and FF values of the cells fabricated with co-evaporated In_2S_3 buffer are significantly lower than those of the other devices fabricated in this work; this behavior seems to be caused by interdiffusion of In_2S_3 into the absorber during its growth, because this layer is deposited around 300^0C, whereas the CBD deposited layers are grown at 70^0C. The interdiffusion of In_2S_3 reduces the shunt resistance of the device and deteriorates the hetero-interface with the CGS absorber; leading to an increase of the interface recombination. The very low Voc and Isc values obtained with solar cells fabricated using co-evaporated In_2S_3 buffer, suggest that the interface recombination is the predominant loss mechanism of photocurrent in this type of devices and the mechanism responsible for the additional reduction of Voc observed in the cells fabricated with co-evaporated In_2S_3 buffer.

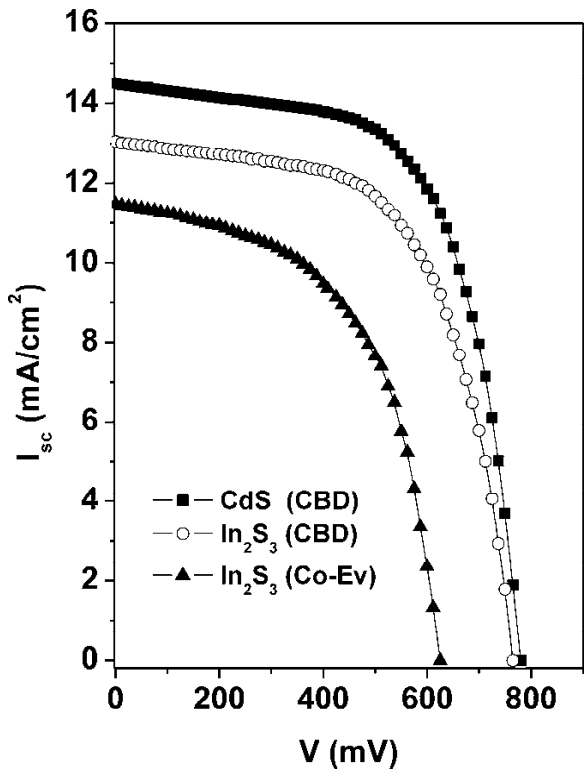

FIG. 11: $J - V$ Characteristics of $CuGaSe_2$/CBD-CdS, $CuGaSe_2$/CBD-In_2S_3 and $CuGaSe_2$/coevaporated-In_2S_3 based solar cells.

4. CONCLUSIONS

Conditions for reproducible deposition of In_2S_3 thin films by CBD with adequate properties to be used as buffer layer in CGS based solar cells were found. XRD studies revealed that the deposition parameters of CBD deposited In_2S_3 films affect the phase in which they grow; on the contrary, the XRD measurements indicated that in the range studied, the co-evaporated In_2S_3 films always grow in the tetragonal $\beta - In_2S_3$ phase, independently of the synthesis parameters used. It was also found that, the substrate type does not affect the phase in which the samples grown. AFM measurements indicated that grain size of In_2S_3 thin films is significantly

TABLE 3: Comparison of the electrical output parameters of CGS solar cells fabricated using CBD and co-evaporated In_2S_3 as buffer, with those of a cell fabricated with CdS buffer.

Cell structure	V_{OC} (mV)	J_{SC} (mA/cm)	FF	η (%)
Mo/CGS/CBD-CdS/ZnO	765	13.1	0.60	7.0
Mo/CGS/CBD-In_2S_3/ZnO	625	11.5	0.55	6.0
Mo/CGS/evap-In_2S_3/ZnO	785	14.5	0.62	3,9

affected by the substrate type and film thickness.

Spectral transmittance measurements revealed that very thin In_2S_3 films deposited by CBD present greater substrate coverage than those of similar thickness deposited by co-evaporation. It leads to building solar cells with higher photocurrent values.

In general, the cells fabricated in this work are characterized by rather low open circuit voltage values, which could be attributed to bulk recombination via states generated by intrinsic defects induced by a lattice mismatch between the surface layer and the bulk material that arises in CGS at a very high density. The results also revealed that the performance of CGS based solar cells fabricated using CBD deposited In_2S_3 buffer layer is similar to reference solar cell fabricated with CBD deposited CdS buffer layer and better than performance obtained with CGS based solar cells fabricated using coevaporation deposited In_2S_3. The best efficiency was 6% for cells with In_2S_3 buffer and 7% for cells with CdS buffer.

Acknowledgements

This work was supported by Colciencias (Contract #247-08) and DIB-Universidad Nacional de Colombia.

[1] I. Repins, M.A. Contreras, B. Egaas, C. DeHart, J. Scharf, C. L. Perkins B. To, R. Noufi. "Short Communication: Accelerated Publication: (199)-efficient ZnO/CdS/$CuInGaSe_2$ solar cell with (812) fill factor". *Progress in Photovoltaics: Research and Applications*, 16, 2008, pp. 235-239.

[2] Naghavi N, C. Hubert, V. Bermudes, B. Cavana, A. Etcheberry, D. Hariskos, M. Powalla, D. Lincot, O. Kerrec, "From CdS to Zn(S,O,OH) : a better understanding of chemical bath deposition parameters and cells properties using electrodeposited $CuIn(S,Se)_2$ and coevaporated $Cu(In,Ga)Se_2$ absorbers". In *21st European Photovoltaic Solar Energy Conference*, Dresden, Germany (2006) 1843.

[3] Ennaoui, A, M. Bar, J. Klaer, T. Kropp, R. Sez-Araos M.C. Lux-Steiner, "New Chemical Route for the Deposition of ZnS Buffer Layers: Cd-free $CuInS_2$-based thin film solar cells with efficiencies above 11%". In *20th European Photovoltaic Solar Energy Conference*, Barcelona, Spain (2005) 1882.

[4] M.A. Contreras, T. Nakada, M. Hongo, O.A. Pudov and J. R. Sites, "$ZnO/ZnS(O,OH)/Cu(In,Ga)Se_2$/Mo solar cell with 18.6% efficiency" *3rd World Conference on Phorovoltaics Energy Conversion, Osaka. Japan (2003)* .

[5] D. Hariskos, S. Spiering, M. Powalla, "Buffer layers in Cu(In,Ga)Se2 solar cells and modules", Thin Solid films 480–481 (2005) 99–109.

[6] D. Hariskos, M. Ruckh, U. Rqhle, T. Walter, H.W. Schock, J. Hedstrfm, L. Stolt, 'A novel cadmium free buffer layer for $Cu(In,Ga)Se_2$ based solar cells', Solar Energy Materials and Solar Cells 41–42 (1996) 345.

[7] A. Ennaoui, S. Siebentritt, M.Ch. Lux-Steiner, W. Riedl, F. Karg, 'High-efficiency Cd-free CIGSS thin film solar cells with solution grown zinc compound buffer layers', Solar Energy Materials and Solar Cells 67 (2001) 31.

[8] S. Chaisitsak, Y. Tokita, H. Miyazaki, R. Mikami, A. Yamada, M., Konagai, 'Control preferred orientation for $Cu(InGa)Se_2$ thin films and its effect on solar cell performance', Proceedings 17th European Photovoltaic Solar Energy Conference, Munich, Germany, 2001, pp. 1011.

[9] E. Romero , J. Clavijo, J.S. Oyola and G. Gordillo, " Effect of synthesis parameters on the optical and structural properties of $CuGaSe_2$ thin films", Rev. Mex. De Física, S 53 (7) (2007) 265-269.

[10] G. Gordillo, F. Mesa and C. Calderón, "Electrical and Morphological Properties of Low Resistivity Mo thin Films Prepared by Magnetron Sputtering", Brazilian Journal of Physics, vol.36 , No.3B (2006) 982-985.

[11] G. Gordillo**,** C. Calderón, J. Olarte y H. Mndez, "Preparation and Characterization of ZnO thin Films deposited by Reactive Evaporation", Proc. 2nd World Conference on Photov. Solar Energy Convertion, Vienna-Austria (1998) pp 750.

[12] M. Froment, D. *Lincot.* 'Phase formation processes in solution at the atomic level: metal chalcogenide semiconductors', *Electrochem. Acta.* 40, (1995) pp. 1293-1303.

[13] C.D. Lockhande, A. Ennaoui, P.S. Patil, M. Giersig, K. Diesner, M. Muller, H. Tributsch, 'Chemical bath deposition of indium sulphide thin films: preparation and characterization', Thin Solid Films 340 (1999) 18.

[14] R. Bayon, J. Herrero: "Structure and morphology of the indium hydroxy sulphide thin films", Appl. Surf. Sci 158 (2009) 49–57.

[15] L. Lyudmila, K. Kim, K. Yoon, M. Konagai, A. Byung. "Thin film CIGS-based solar cells with an In-based buffer layer fabricated by chemical bath deposition", *3rd World Conference on Photovoltaics Energy Conversion, Osaka. Japan (2003).*

[16] R Swanepoel 'Determination of the thickness and optical constants of amorphous silicon'. J. Phps. E: Sci. Instrum.. Vol. 16, 1983.

[17] M.A Contreras, H. Wisner, J. Tuttle, K. Ramanathan and R. Noufi, "Issues of the chalcopyrite/defect-chalcopyrite junction model for high-efficiency $Cu(In,Ga)Se_2$ solar cells", Solar Energy Mat. Solar Cells 49 (1997) 239-247.

[18] M.D. Archer and R. Hill (Editors), "Clean electricity from photovoltaics". Imperial College Press, London. 2001.